

Localized FNO for Spatiotemporal Hemodynamic Upsampling in Aneurysm MRI

Kyriakos Flouris^{*1[0000-0001-7952-1922]}, Moritz Halter^{*1}, Yolanne Y. R. Lee², Samuel Castonguay³⁴, Luuk Jacobs⁵, Pietro Dirix⁵, Jonathan Nestmann⁵, Sebastian Kozerke⁵, and Ender Konukoglu¹

¹ Biomedical Imaging Group, Computer Vision Lab, ETH Zurich
{kflouris;mhalter,kender}@ethz.ch

² Department of Computer Science, University College London
yolanne.lee.19@ucl.ac.uk

³ Institute of Environmental Engineering, Swiss Federal Institute of Technology, ETH Zurich

⁴ Biodiversity and Conservation Biology Unit, Swiss Federal Institute for Forest, Snow and Landscape Research, WSL

⁵ Institute for Biomedical Engineering, University and ETH Zurich

Abstract. Hemodynamic analysis is essential for predicting aneurysm rupture and guiding treatment. While magnetic resonance flow imaging enables time-resolved volumetric blood velocity measurements, its low spatiotemporal resolution and signal-to-noise ratio limit its diagnostic utility. To address this, we propose the Localized Fourier Neural Operator (LoFNO), a novel 3D architecture that enhances both spatial and temporal resolution with the ability to predict wall shear stress (WSS) directly from clinical imaging data. LoFNO integrates Laplacian eigenvectors as geometric priors for improved structural awareness on irregular, unseen geometries and employs an Enhanced Deep Super-Resolution Network (EDSR) layer for robust upsampling. By combining geometric priors with neural operator frameworks, LoFNO de-noises and spatiotemporally upsamples flow data, achieving superior velocity and WSS predictions compared to interpolation and alternative deep learning methods, enabling more precise cerebrovascular diagnostics. The code, ablations and hyperparameters are available at: <https://github.com/moritz-halter/deepflow>.

Keywords: 4D flow MRI · Super-resolution · Hemodynamics · Aneurysm

1 Introduction

Intracranial aneurysms (IAs) and arteriovenous malformations (AVMs) are major causes of hemorrhagic strokes, leading to significant morbidity and mortality [23]. Timely surgical or endovascular interventions are critical to reducing rupture risk and preventing cerebral hemorrhage in high-risk individuals [3, 20].

* These authors contributed equally to this work.

Accurate diagnostic imaging is essential for identifying at-risk patients, assessing disease severity, and guiding treatment planning [17, 8].

Current clinical imaging primarily captures morphological data, often overlooking hemodynamic parameters that could enable earlier rupture prediction [7, 19]. Hemodynamic analyses based solely on morphology rely on costly computational fluid dynamics (CFD) simulations or simplified models derived from limited imaging slices, which may not fully capture the complexity of cerebral blood flow [16]. Recent advances in 4D flow magnetic resonance (MR) imaging now allow time-resolved volumetric measurements of blood velocity vector fields throughout the brain [18], providing real data that was previously only available through CFD simulations. These measurements enable detailed flow pattern analyses, collateral flow activation, arterial and venous pulsatility, pressure gradients, and wall shear stress (WSS), aiding in the detection and diagnosis of IA [29]. While 4D flow MR imaging eliminates the computational burden of CFD and the labor-intensive construction of geometric models, its low spatiotemporal resolution and signal-to-noise ratio remain major limitations. Interpolation methods can improve resolution, but they require manual selection of methods and parameters for each case, limiting automation and scalability.

Neural networks are widely used for medical image upsampling, with models like Enhanced Deep Super-Resolution Network (EDSR)[13] excelling in single-image super-resolution. However, the anatomical variability of IA complicates both upsampling and clinical tasks like diagnosis and rupture prevention[29]. Beyond image enhancement, neural networks have been explored for predicting hemodynamic parameters directly from imaging data, bypassing the computational bottlenecks of CFD. However, solving temporal dynamics and medical imaging super-resolution remains an open challenge.

We propose a novel, domain-agnostic Fourier Neural Operator (FNO) architecture, Localized Fourier Neural Operator (LoFNO), which incorporates embeddings of Laplacian eigenvectors to enhance geometric awareness [14]. Designed to both upsample spatial resolution and temporal dynamics, enabling the prediction of intermediate time steps from sparse inputs. LoFNO predicts hemodynamic parameters directly from routinely acquired flow from MR imaging data, providing an efficient alternative to traditional CFDs.

Our approach introduces three key contributions: (1) integrating *Laplacian eigenvectors* as geometric priors to improve generalization across irregular vascular geometries, (2) incorporating an *EDSR-based super-resolution layer* to enhance image quality and robustness to noise, and (3) implementing LoFNO on a synthetic 4D flow IA dataset. Real data analysis is not feasible due to the need for high-quality training flow and geometry data, as obtaining very high-resolution 4D flow MRI is highly impractical. However, once trained, the model can be used to upsample low-resolution flow data, making it more applicable in a clinical setting. Fig. 1 outlines the complete pipeline, from aneurysm extraction and CFD data preparation to flow parameters prediction.

Relevant Works Deep neural networks are widely used for upsampling and super-resolution [5, 9, 25], with Super-Resolution Convolutional Neural Network

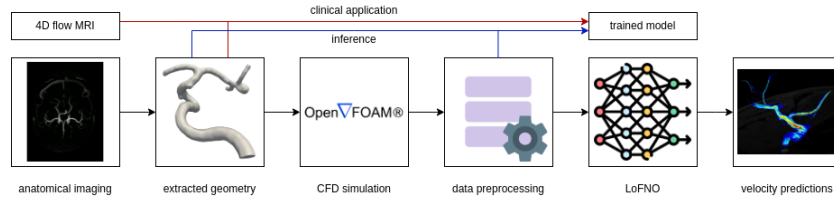


Fig. 1. Method pipeline: Geometry and boundary conditions are extracted from cerebral angiograms. Simulations are run, the relevant section is segmented, Laplacian eigenvectors are computed, and noise is added. Flow and eigenvectors are sampled on a voxel grid for preprocessing. The model is trained to predict noise-free flow on a high-resolution grid and tested on unseen data. In clinical use, it can be applied directly to 4D flow MRI *without* CFD simulations.

(SRCNN) [4] and EDSR [13] playing key roles. Physics-informed methods integrate physical priors into training, including Physics-Informed Neural Network (PINN)s [2] and other specialized frameworks [15, 24, 6]. While effective, these methods struggle with fixed discretization when solving continuous equations and face challenges in enforcing boundary conditions on complex geometries.

Domain Agnostic Fourier Neural Operator (DAFNO)[14] and Geo-FNO[11] aim to alleviate the constraint of operator methods on fixed geometries by enabling applications to general geometries, while Incremental FNO [28] introduces adaptive training schedules to improve efficiency. Despite these advances, generalization to unseen geometries remains challenging, as these methods were not originally designed for intricate biological boundaries such as those in aneurysms.

There are numerous techniques that leverage spectral coordinates for geometric processing [10] [22], based on geometric deep learning [1]. In this work, we introduce a novel architecture that builds upon DAFNO, leveraging spectral embeddings [1] [10] and incorporating EDSR to efficiently upsample the spatial and temporal resolution of 4D flow imaging.

2 Method

The LoFNO consists of an EDSR module that takes low-resolution flow data and Laplacian eigenvectors as input, refining spatiotemporal resolution while integrating geometric features from spectral coordinates. The output, is then processed by a DAFNO layer with implicit FNOs, where a domain characteristic function ensures computations remain localized to the aneurysm geometry.

Operator methods enable learning generalized physical models across diverse domains. We aim to learn a mapping $\hat{G} : \mathcal{A} \rightarrow \mathcal{U}$, where $\mathcal{A}(\mathbb{R}^{d_{in}})$ represents input velocity fields $u_i(x)$ and $\mathcal{U}(\mathbb{R}^{d_{out}})$ represents high-resolution output velocity fields $\hat{u}_i(x)$ over a patient-specific aneurysm domain $\Omega_i \subset \mathbb{R}^3$. This mapping is parameterized by θ and trained to approximate $\hat{G}[u_i; \theta](x) \approx \hat{u}_i(x), \forall x \in \Omega_i$.

Unlike traditional neural networks, the Neural Operator (NO) maintains discretization invariance, allowing evaluation at arbitrary resolutions.

The FNO [12] leverages Fourier transforms for efficient modeling of spatial dependencies in partial differential equations. It applies a convolution-based layer where a tensor kernel $\kappa \in \mathbb{R}^{d_h \times d_h}$ with parameters v^l operates over the computational domain $\bar{\Omega}$, which contains the aneurysm geometry Ω . By utilizing the Fourier transform \mathcal{F} and its inverse \mathcal{F}^{-1} , FNO exploits the efficiency of Fast Fourier Transform (FFT)/inverse Fast Fourier Transform (iFFT). However, it requires inputs on a regular grid, making it unsuitable for irregular aneurysm geometries. To address this, a periodic domain grid \mathbb{O} is overlaid onto $\bar{\Omega}$, enabling Fourier-based computations but it has limited effectiveness.

Localizing to the Relevant Domains and Geometric Prior Mapping the aneurysm geometry Ω to the grid \mathbb{O} introduces out-of-domain voxels in $\mathbb{O} \setminus \Omega$, increasing complexity and computational inefficiency. These out-of-domain voxels are trivial and detract from the solution, particularly as boundary nodes are crucial for calculating WSS. DAFNOs [14] extend FNO to improve generalization across unseen domains while reducing computational overhead from $\mathbb{O} \setminus \Omega$.

To enforce domain localization, $\chi(x)$ is defined as $\chi(x) = 1$ for $x \in \Omega$ and $\chi(x) = 0$ for $x \in \mathbb{O} \setminus \Omega$. The Fourier layer is modified to ensure interactions remain within the physical domain, Ω , while preserving FFT efficiency. The operator is expressed compactly as:

$$\mathcal{J}^l[h](x) = \sigma\left(\chi(x) \left(I(\chi(\cdot)h(\cdot); v^l) - h(x)I(\chi(\cdot); v^l)\right) + W^l h(x) + c^l\right),$$

where $I(\cdot; v^l) = \mathcal{F}^{-1}[\mathcal{F}[\kappa(\cdot; v^l)] \cdot \mathcal{F}[\cdot]]$ represents the Fourier-based integral computation. $W^l \in \mathbb{R}^{d_h \times d_h}$ and $c^l \in \mathbb{R}^{d_h}$ are learnable parameters. This ensures domain-specific relevance while leveraging FFT for efficient evaluation. Additionally, we adopt implicit FNOs [27], making learnable parameters layer-independent to mitigate overfitting and vanishing gradients.

To map the trained solution to complex and unseen geometries, we use *spectral coordinates*. Laplacian eigenvectors are computed on a graph $\mathcal{G} = (\mathcal{V}, \mathcal{E})$, where \mathcal{V} is the set of vertices and \mathcal{E} the edges. The adjacency matrix $A \in \mathbb{R}^{N \times N}$ encodes connectivity, with $A_{ij} = 1$ if vertices i and j are connected, and the diagonal degree matrix D has D_{ii} as the vertex degree. The normalized graph Laplacian is defined as $L^{\text{sym}} = I - (D^+)^{1/2} A (D^+)^{1/2}$, where I is the identity matrix and D^+ the Moore-Penrose pseudoinverse. Eigenvectors \mathbf{v}_i and eigenvalues λ_i are obtained from $L^{\text{sym}} \mathbf{v}_i = \lambda_i \mathbf{v}_i$, with eigenvalues sorted in descending order. The first $k = 32$ eigenvectors, corresponding to the largest nonzero eigenvalues, capture key geometric features and are normalized as $\mathbf{v}_i \leftarrow \mathbf{v}_i / \|\mathbf{v}_i\|_2, \forall i$.

Enhanced architecture Inspired from SRNO [26], our approach first increases the resolution of the input data to prepare it for the Fourier layers. Instead of interpolation, we use an EDSR network, designed for single-image super-resolution, leveraging convolutional layers and residual connections to handle

noise in the input flow velocity data $u(x)$ sampled on a $d_x \times d_y \times d_z$ grid. This learnable upsampling improves resolution while reducing noise.

The EDSR network takes as input the low-resolution flow velocity data concatenated with the selected eigenvectors $e(x)$ of the Laplacian operator. It outputs a high-resolution representation, which, along with the domain characteristic function $\chi(x)$, is fed into the DAFNO. Within DAFNO, the input is lifted by an multilayer perceptron (MLP) layer P , then processed through Fourier layers, where FFT, matrix multiplications with learnable parameters v^l , and nonlinear activations σ are applied. The characteristic function $\chi(x)$ ensures domain-aware computations by restricting operations to relevant regions.

Finally, the output from the Fourier layers is projected to the target space through another MLP layer Q , reducing dimensionality and producing the noiseless flow velocity prediction $\hat{u}(x)$. See Fig. 2 for a detailed schematic of the LoFNO architecture.

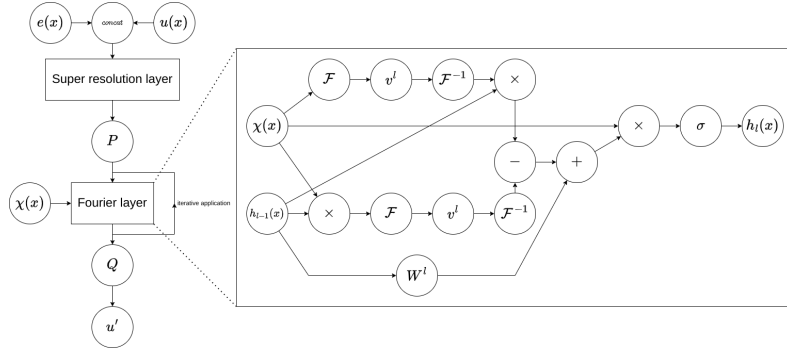


Fig. 2. Computational graph for LoFNO. Both $e(x)$, a selection of eigenvectors, and $u(x)$, the flow velocity with added noise, are sampled on a regular grid, while $\hat{u}(x)$ (prediction for noiseless flow), $\chi(x)$ (domain characteristic function), and $h_l(x)$ (Fourier layer input/output, $l \in \{0, \dots, L\}$) are sampled on a higher resolution grid. The lifting layer P and projection layer Q are MLPs, mapping $(3 + N_e)$ to d_h and d_h to 3, respectively, where N_e is the number of eigenvectors and d_h the Fourier layer dimensionality. Nodes \mathcal{F} and \mathcal{F}^{-1} perform FFT and iFFT, while v^l applies matrix multiplication selecting the first N_m modes for each dimension. The node W^l performs pointwise multiplication with $W^l \in \mathbb{R}^{d_h \times d_h}$, and $+$, $-$, \times , and σ perform pointwise addition, subtraction, multiplication, and activation, respectively. The architecture and hyperparameters were optimized via ablation studies.

3 Experiments and Results

The Blood flow in the vessels was simulated by solving the three-dimensional, unsteady, incompressible Navier–Stokes equations. The blood was modeled as a Newtonian, incompressible fluid with a density of 1060 kg/m^3 and a kinematic

viscosity of $3.5 \times 10^{-3} \text{ Pa} \cdot \text{s}$. In this study, the Navier–Stokes equations were solved using a large eddy simulation (LES) approach implemented in OpenFOAM v2212. The wall-adapting local eddy viscosity (WALE) model was chosen as the subgrid-scale model. Second-order central difference and backward Euler schemes were used for spatial and temporal discretization respectively. An adaptive time-stepping strategy was employed to optimize simulation efficiency.

Using these simulations, we have carried out two sets of experiments, the spatial super-resolution and temporal upsampling. We generated a dataset of 95 pulse flows imposed on geometries from the Aneurisk dataset [21]. The dataset contains 3D reconstructions of internal carotid arteries and their associated aneurysms from cerebral angiographies. Simulations provided detailed hemodynamic parameters, including flow velocity, pressure, and WSS, capturing the complex fluid dynamics within patient-specific vascular geometries. Testing was performed on an unseen subset of geometries and their respective eigenvectors.

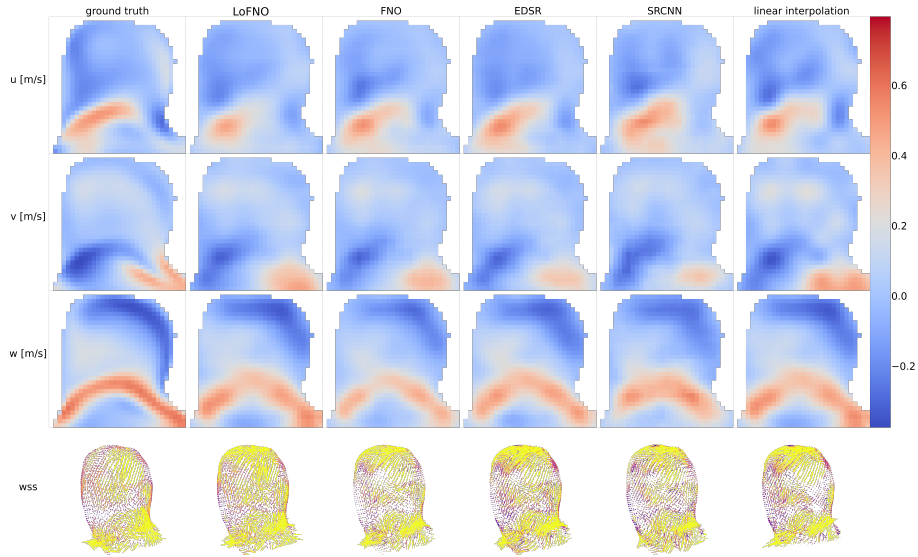


Fig. 3. Time-snapshot of hemodynamics upsampling for Scale $\times 4$: Top: Flow velocity components u , v , and w in the x , y , and z directions for five models compared against the ground truth. Bottom: WSS evaluated on the surface geometry, with the length of vectors colored black for the smallest to yellow for the largest.

We selected 80 aneurysm-containing regions, computed Laplacian eigenvectors on the surface mesh, and resampled them onto a Cartesian grid using VTK’s `vtkResampleWithDataSet`. Interior vessel points within subdomain Ω were marked, and white noise with a signal-to-noise ratio of 10 was added. Enforcing divergence-free interpolation was omitted as it caused artifacts, likely due to an overdetermined system from fixed points and the divergence-free con-

straint. Laplacian eigenvalues were computed on the VTK mesh, defining the graph, and resampled to the grid using point interpolation via `vtkPointInterpolator` with a Gaussian kernel to preserve boundary information.

We trained several deep learning models, including SRCNN, EDSR, FNO, and the proposed LoFNO, conducting experiments. Additionally, we evaluated classical interpolation methods such as Radial Basis Function (RBF) interpolation, Data-Driven Flow Interpolation (DFI), and linear interpolation. While PINNs performed well with sparse data, they exhibited instability with denser inputs and proved inefficient for large 3D datasets, thus not included.

Models were trained for 500 epochs, reaching near convergence. For spatial upsampling, models reconstructed a noiseless high-resolution flow field of either 32^3 or 24^3 from noisy low-resolution inputs of 16^3 or 8^3 , obtained by subsampling the high-resolution data across all 24 timesteps. For temporal upsampling, models reconstructed a full high-resolution $32^3 \times 24$ flow field from noisy, high-spatial-resolution but temporally undersampled inputs, including $32^3 \times 12$, $32^3 \times 6$, and $32^3 \times 1$, where for the latter the entire sequence was predicted from the initial timestep only. For all models, we minimized the relative loss $= \sum_{x \in \mathcal{O}} \sum_t |u(x, t) - \hat{u}(x, t)| / |u(x, t)|$, where $u(x, t)$ is the ground truth flow velocity and $\hat{u}(x, t)$ the predicted velocity at spatial point x and time t .

Results For testing, we use a subset of 10 geometries that were unseen during training. The predicted results for the best-performing methods are shown in Fig. 3. While none of the methods achieved perfect reconstruction, as expected given the complexity of the problem and the unseen geometries, LoFNO qualitatively demonstrated better performance than the other methods in reconstructing velocities and WSS.

To evaluate model performance more concretely, we define the error function as $\text{err}f(x, t) = \|f(x, t) - \hat{f}(x, t)\|_2$, which can be applied to flow velocity $u(x, t)$ or WSS. Each model is benchmarked by averaging the error over all spatial and temporal dimensions across the test set. The differences are highlighted in the quantitative comparison in Table 1, where complete LoFNO outperformed other approaches, underscoring the significance of domain and geometric priors.

Table 1. Test-error, L^{test} , for hemodynamics parameters upsampling.

Model	Scale $\times 4$		Scale $\times 3$		Scale $\times 2$		Training / Evaluation
	u	wss	u	wss	u	wss	
Linear Interp.	0.0684	1.0914	0.04661	0.5680	0.0497	0.8366	$na/ < 1$ min
RBF Interp.	0.0813	1.4261	0.0563	0.6886	0.0591	0.9387	$na/ \sim 15$ min
DFI Interp.	0.2054	2.8680	0.1339	1.3554	0.1864	2.5229	$na/ \sim 1$ h
SRCNN	0.0807	1.1081	0.0574	0.6527	0.0389	0.7969	~ 15 min/ ~ 10 s
EDSR	0.0683	1.1483	0.0460	0.5840	0.0300	0.6265	~ 15 min/ ~ 10 s
FNO [§]	0.0647	0.9832	0.0388	0.4529	0.0272	0.5288	~ 1 h/ ~ 10 s
LoFNO <i>wo</i> LEP ¶	0.0464	0.7699	0.0292	0.3750	0.0201	0.4220	~ 1 h/ ~ 10 s
LoFNO	0.0452	0.7625	0.0291	0.3637	0.0198	0.4139	~ 1 h/ ~ 10 s

Combining neural operators with super-resolution networks yielded significant gains, as seen by the $\sim 25\%$ achieved by the LoFNO *wo* LEP. The results are improved with the addition of the Laplacian eigenvectors as geometric priors. Noteworthily, not only does LoFNO improve on the aggregated metrics, but the results consistently outperform the other methods for every individual test case. The localized geometry nature of our framework enhanced robustness and adaptability. While all methods train efficiently on modern hardware, interpolation techniques are slower during evaluation. We have also trained and tested on noiseless data, yielding similar trends, but omitted it due to limited real-world applicability.

Table 2. Test-error, L^{test} , for hemodynamics parameters temporal upsampling.

Model	Scale $\times 2$		Scale $\times 4$		Prediction		Training / Evaluation
	u	wss	u	wss	u	wss	
Linear Interp.	0.0632	0.5631	0.0699	0.6107	0.1145	0.9520	$na/ < 1$ min
SRCNN	0.0461	0.7141	0.0607	0.8298	0.0600	0.8082	~ 15 min/ ~ 10 s
EDSR	0.0317	0.4689	0.0459	0.5765	0.0624	0.7671	~ 15 min/ ~ 10 s
FNO [§]	0.0384	0.4367	0.0382	0.4247	0.0678	0.7546	~ 1 h/ ~ 10 s
LoFNO <i>w/o</i> LEP [¶]	0.0245	0.2987	0.0315	0.3684	0.0531	0.6028	~ 1 h/ ~ 10 s
LoFNO	0.0195	0.2723	0.0280	0.3424	0.0536	0.5941	~ 1 h/ ~ 10 s

For temporal super-resolution, our model showed even greater improvements, as seen in Table 2. Even standalone FNO performed well across all tested scales. However, despite full spatial resolution being available, augmenting FNOs with domain or geometric priors, such as the domain characteristic function and Laplacian eigenvectors i.e. the LoFNO, further enhanced performance.

The complete prediction task, $32^3 \times 1$ to $32^3 \times 24$, where 23 future time steps are predicted from a single initial one, is particularly challenging. Despite this, all machine learning models, and especially our method, maintained reasonable accuracy, while interpolation methods suffered a severe performance drop. Even with an extra 25^{th} time step, interpolation remained far less accurate. This disparity arises because the CFD simulation applies the same pressure pulse at the vessel inlet. Machine learning models, trained on slight pulse variations, effectively captured the underlying dynamics, enabling accurate predictions even on unseen geometries. In contrast, interpolation methods, lacking system knowledge, relied only on given data points, limiting their predictive capability.

Limitations While LoFNO offers efficiency and scalability, it depends on CFD data for training, as no real data exist for this task, which may not capture real-world variability. These methods also lack inherent temporal mechanisms, limiting interpretability for dynamic flow modeling. We evaluated several super-

[§] A FNO with a preceding EDSR layer

[¶] LoFNO without Laplacian Eigenvalues Prior (LEP)

resolution alternatives and found that the chosen methods, including the gold standard FNO, consistently matched or outperformed others. We were also constrained to methods that could be adapted to large 3D datasets.

4 Conclusions

We proposed LoFNO, a novel architecture that outperforms interpolation and alternative methods in test-error for spatial and temporal upsampling of velocity and WSS predictions. Our focus in this work is to address a key methodological challenge: super-resolving fluid dynamics variables in complex boundaries remains unsolved, even with large-scale, high-fidelity simulated data. Generalizing to unseen geometries is not only relevant to aneurysms but to many other problems. The proposed model directly targets this. To demonstrate its effectiveness, we focus on quantitative evaluation using high-resolution simulated data, where ground truth is available. This assessment would not have been possible with clinical data because the ground truth cannot be easily acquired. By enabling precise, non-invasive prediction of hemodynamic parameters, LoFNO can improve clinical assessment, enhance disease progression predictions, and optimize therapeutic outcomes, ultimately advancing patient care and safety.

References

1. Bronstein, M.M., Bruna, J., Cohen, T., Velickovic, P.: Geometric deep learning: Grids, groups, graphs, geodesics, and gauges. CoRR **abs/2104.13478** (2021), <https://arxiv.org/abs/2104.13478>
2. Cai, S., Mao, Z., Wang, Z., Yin, M., Karniadakis, G.E.: Physics-informed neural networks (pinns) for fluid mechanics: A review. *Acta Mechanica Sinica* **37**(12), 1727–1738 (2021)
3. Deshmukh, A.S., Priola, S.M., Katsanos, A.H., Scalia, G., Costa Alves, A., Srivastava, A., Hawkes, C.: The management of intracranial aneurysms: Current trends and future directions. *Neurology International* **16**(1), 74–94 (2024)
4. Dong, C., Loy, C.C., He, K., Tang, X.: Image super-resolution using deep convolutional networks. *IEEE transactions on pattern analysis and machine intelligence* **38**(2), 295–307 (2015)
5. Flouris, K., Konukoglu, E.: Canonical normalizing flows for manifold learning. In: Oh, A., Naumann, T., Globerson, A., Saenko, K., Hardt, M., Levine, S. (eds.) *Advances in Neural Information Processing Systems*. vol. 36, pp. 27294–27314. Curran Associates, Inc. (2023)
6. Flouris, K., Volokitin, A., Bredell, G., Konukoglu, E.: Explicit and data-efficient encoding via gradient flow (2025), <https://arxiv.org/abs/2412.00864>
7. Han, P., Jin, D., Wei, W., Song, C., Leng, X., Liu, L., Yu, J., Li, X.: The prognostic effects of hemodynamic parameters on rupture of intracranial aneurysm: A systematic review and meta-analysis. *International Journal of Surgery* **86**, 15–23 (2021)
8. Hussein, A., Malguria, N.: Imaging of vascular malformations. *Radiologic Clinics* **58**(4), 815–830 (2020)

9. Ledig, C., Theis, L., Huszár, F., Caballero, J., Cunningham, A., Acosta, A., Aitken, A., Tejani, A., Totz, J., Wang, Z., Shi, W.: Photo-realistic single image super-resolution using a generative adversarial network. In: 2017 IEEE Conference on Computer Vision and Pattern Recognition (CVPR). pp. 105–114 (2017)
10. Li, X.J., Yang, J., Zhang, F.L.: Laplacian mesh transformer: Dual attention and topology aware network for 3d mesh classification and segmentation. In: Avidan, S., Brostow, G., Cissé, M., Farinella, G.M., Hassner, T. (eds.) *Computer Vision – ECCV 2022*. pp. 541–560. Springer Nature Switzerland, Cham (2022)
11. Li, Z., Huang, D.Z., Liu, B., Anandkumar, A.: Fourier neural operator with learned deformations for pdes on general geometries. *Journal of Machine Learning Research* **24**(388), 1–26 (2023)
12. Li, Z., Kovachki, N., Azizzadenesheli, K., Liu, B., Bhattacharya, K., Stuart, A., Anandkumar, A.: Fourier neural operator for parametric partial differential equations (2021)
13. Lim, B., Son, S., Kim, H., Nah, S., Mu Lee, K.: Enhanced deep residual networks for single image super-resolution. In: *Proceedings of the IEEE conference on computer vision and pattern recognition workshops*. pp. 136–144 (2017)
14. Liu, N., Jafarzadeh, S., Yu, Y.: Domain agnostic fourier neural operators. *Advances in Neural Information Processing Systems* **36** (2024)
15. Liu, X.Y., Zhu, M., Lu, L., Sun, H., Wang, J.X.: Multi-resolution partial differential equations preserved learning framework for spatiotemporal dynamics. *Communications Physics* **7**(1) (Jan 2024)
16. Maramkandam, E.B., Kannan, A., Valeti, C., Manjunath, N., Panneerselvam, N.K., Alagan, A.K., Panchal, P.M., Kannath, S.K., Darshan, H., Nekkanti, R.K., et al.: Review of cfd based simulations to study the hemodynamics of cerebral aneurysms. *Journal of the Indian Institute of Science* pp. 1–34 (2024)
17. Maupu, C., Lebas, H., Boulaftali, Y.: Imaging modalities for intracranial aneurysm: more than meets the eye. *Frontiers in Cardiovascular Medicine* **9**, 793072 (2022)
18. Morgan, A.G., Thrippleton, M.J., Wardlaw, J.M., Marshall, I.: 4d flow mri for non-invasive measurement of blood flow in the brain: a systematic review. *Journal of Cerebral Blood Flow & Metabolism* **41**(2), 206–218 (2021)
19. Nico, E., Hossa, J., McGuire, L.S., Alaraj, A.: Rupture-risk stratifying patients with cerebral arteriovenous malformations using quantitative hemodynamic flow measurements. *World Neurosurgery* **179**, 68–76 (2023)
20. Pan, P., Weinsheimer, S., Cooke, D., Winkler, E., Abla, A., Kim, H., Su, H.: Review of treatment and therapeutic targets in brain arteriovenous malformation. *Journal of Cerebral Blood Flow & Metabolism* **41**(12), 3141–3156 (2021)
21. Sangalli, L.M., Secchi, P., Vantini, S.: AneuRisk65: A dataset of three-dimensional cerebral vascular geometries. *Electronic Journal of Statistics* **8**(2), 1879 – 1890 (2014)
22. Torres, L., Chan, K.S., Eliassi-Rad, T.: GLEE: Geometric laplacian eigenmap embedding. *Journal of Complex Networks* **8**(2), cnaa007 (Mar 2020)
23. Van Gijn, J., Kerr, R.S., Rinkel, G.J.: Subarachnoid haemorrhage. *The Lancet* **369**(9558), 306–318 (2007)
24. Wang, R., Kashinath, K., Mustafa, M., Albert, A., Yu, R.: Towards physics-informed deep learning for turbulent flow prediction (2020)
25. Wang, Y., Lee, Y.Y.R., Dolfini, A., Reischl, M., Konukoglu, E., Flouris, K.: Energy-based prior latent space diffusion model for reconstruction of lumbar vertebrae from thick slice mri. In: Mukhopadhyay, A., Oksuz, I., Engelhardt, S., Mehrof, D., Yuan, Y. (eds.) *Deep Generative Models*. pp. 22–32. Springer Nature Switzerland, Cham (2025)

26. Wei, M., Zhang, X.: Super-Resolution Neural Operator . In: 2023 IEEE/CVF Conference on Computer Vision and Pattern Recognition (CVPR). pp. 18247–18256. IEEE Computer Society, Los Alamitos, CA, USA (Jun 2023)
27. You, H., Zhang, Q., Ross, C.J., Lee, C.H., Yu, Y.: Learning deep implicit fourier neural operators (ifnos) with applications to heterogeneous material modeling. *Computer Methods in Applied Mechanics and Engineering* **398**, 115296 (2022)
28. Zhao, J., George, R.J., Zhang, Y., Li, Z., Anandkumar, A.: Incremental fourier neural operator. arXiv preprint arXiv:2211.15188 (2022)
29. Zhou, G., Zhu, Y., Yin, Y., Su, M., Li, M.: Association of wall shear stress with intracranial aneurysm rupture: systematic review and meta-analysis. *Scientific Reports* **7**(1), 5331 (2017)